Artificial Life and Robotics
https://doi.org/10.1007/s10015-020-00610-w

ORIGINAL ARTICLE

Analysis of body undulation using dynamic model with frictional force for myriapod robot

Naoki Miyamoto[1] · Tetsuya Kinugasa[1] · Tatsuya Amasaki[1] · Koichi Osuka[2] · Ryota Hayashi[1] · Koji Yoshida[1]

Received: 3 February 2020 / Accepted: 22 May 2020

Abstract
Myriapoda, having multitudes of legs and an elongated body, can dexterously travel on natural environments. Myriapod locomotion has an advantage over wheeled and tracked vehicles on a rough terrain, because each leg can discretely contact the ground at several points. The authors have attempted, therefore, to develop a light, simple, and adaptive myriapod robot, i-CentiPot, in accordance with the implicit control law given by passive dynamics, which achieved significant mobility against unpredictable environment. The physical model, i-CentiPot 01, showed that the body undulation emerged because of the leg wave, which was similar to that of a real centipede. However, the mechanism of the body undulation was not revealed. This study, therefore, aims at developing a dynamic model of the myriapod robot using frictional force and elucidating how it locomotes.

Keywords Myriapod robot · Passive dynamics · Dynamic model · Frictional force

1 Introduction

Myriapoda are characterized by their multitudes of legs and an elongated bodies that allow them to dexterously travel on their natural environments. Myriapod locomotion has an advantage over wheeled and tracked vehicles on a rough terrain, because each leg can discretely contact the ground at several points. Nonetheless, only a few studies (e.g., [1, 2]) have been done in the field of physiology to reveal the mechanisms of the multi-legged locomotion. For example, Anderson et al. [2] observed the electromyograms (EMGs) of muscles of centipede *Scolopendra heros*. The EMGs showed muscle activity synchronization via the posteriorly propagated waves caused by bending. The velocities and magnitudes of the waves propagating along the body were observed to increase when the forward velocity of the centipede increased. To further investigate myriapod locomotion, a synthetic approach [3, 7–9], i.e., making a robot to understand intelligence, is focused on. Previous myriapod robots, however, were originally created to be large and heavy to actuate numerous joints, and thus, it was difficult for the robots to be able to synthesize aspects of the intelligence, such as adaptability to natural environments, of Myriapoda. For a simple configuration, Saranli et al. [5], for example, proposed a hexapod robot with a revolvable leg that achieved high mobility. On the other hand, Koh et al. developed a lightweight and simple 24-leg robot [4]. The interests of these studies, however, were not in the synthesis of creature behavior, but in the development of robots with high mobility. Meanwhile, Hoffman developed and analyzed a tiny centipede robot with active legs and passive body joints [6], and found some undulatory gait similar to that of a centipede, which improved speed for traveling. The result followed the finding of Anderson et al. To achieve significant mobility against unpredictable environments, we have attempted to develop a light, simple, and adaptive myriapod robot, which we called the i-CentiPot (Fig. 1), in accordance with the implicit control law given by passive dynamics [12]. The physical model, i-CentiPot 01, revealed that body undulation emerged because of the leg wave propagating posteriorly, which was similar to in a real centipede [13].

This work was presented in part at the 25th International Symposium on Artificial Life and Robotics, Beppu, Oita, January 22–24, 2020, and supported by CREST, JST, and JSPS KAKENHI No. 17K06281.

✉ Naoki Miyamoto
gundameki@gmail.com

[1] Okayama University of Science, Okayama, Japan

[2] Osaka University and JST CREST, Osaka, Japan

Published online: 11 July 2020

Fig. 1 Myriapod robot, i-CentiPot 01

Fig. 2 Lateral undulation of body with retrograde wave for i-CentiPot 01 (above) and a centipede (below). The pair of legs was 180° out of phase

However, the aspect of the passive undulation with respect to frequency of the legs was not revealed.

This study, therefore, aims at developing a dynamic model of the myriapod robot using frictional force and elucidating how it locomotes. First, a dynamic model comprising a body and N pairs of legs is derived. The propulsive force is created by a frictional forces developing at every tip of the leg. The friction model is expected to prevent unnatural movement because it allows for slippage to occur for large forces on the leg tip. We then conduct some numerical simulations to demonstrate that the dynamic model can locomote. Finally, we analyze the body undulation with respect to leg frequency. For the physical model, i-CentiPot, the legs contacting the ground, which provided propulsive force, are placed in the concave side of each bent region when it locomotes. We also confirm that the dynamic model emerges with a similar body undulation for some appropriate leg frequency. However, we also find that the relationship between the body undulation and the leg wave varied with respect to the leg frequency. Indeed, the convex area of the body follows the same direction of the ground contact area of leg tips for some leg frequency.

2 Lateral undulation of body

Here, the body undulation of the i-CentiPot is briefly introduced [13]. Figure 2 (above) shows a locomoting i-CentiPot 01. In this case, the foot wave propagates from head to tail, i.e., the feet provide a retrograde wave. The red ellipsoids indicates areas of ground contact, where several feet concentrate. We can find that the body segments with the feet inside the ellipsoid move in a convex manner to the opposite side of the contacted feet. The undulation of the body caused by the retrograde wave of the feet is analogous to that of a centipede, as shown in Fig. 2 (below).

3 Dynamic model

For the analysis of the body undulation, a dynamic model is first derived. We assume that the motion of the myriapod is planar, i.e., the model does not roll. Each pair of left and right legs is modeled by one link. As shown in Fig. 3, the model comprises $2N$ links, each of which is either an the odd link, a $(2i-1)$th link $(i = 1, ..., N)$, which refers to a body segment, or an even link, a $2i$th link, which refers to a pair of legs. The first link represents the rear end, whereas the $(2N-1)$th link represents the front body segment. Let l_{b_i} be the length of the ith body segment, or the $(2i-1)$th link, and l_{l_i} be the length of the ith pair of legs, or the $2i$th link. Let m_{b_i} and m_{l_i}, and $I^G_{b_i}$ and $I^G_{l_i}$ be the corresponding masses and inertial moments about the center of mass (CoM), respectively, of the ith link. Each body segment has a pair of legs, where each leg is connected to the center of the body segment.

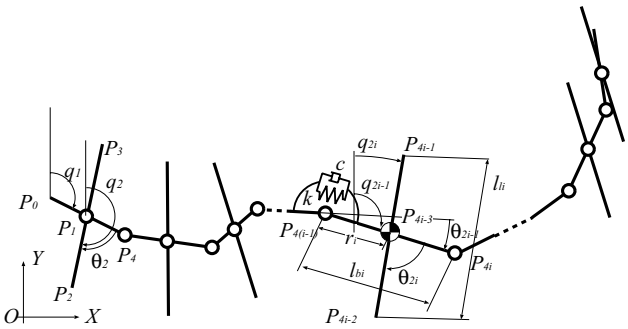

Fig. 3 Link model

3.1 Equation of motion

The generalized coordinate is given as $q = [q_1, ..., q_{2N}, P_0^T]^T \in R^{(2N+2)\times 1}$, where $P_0 = [x_0, y_0]^T \in R^{2\times 1}$ is the rear end position and q is the absolute angle of each link. Each CoG position of body segment $P_{g_{2i-1}}$ and pair of leg $P_{g_{2i}}$ corresponding to P_{4i-3} shown in Fig. 3 is given by the following equation:

$$P_{g_{2i-1}} = P_{g_{2i}} = P_{4(i-1)} + r_i[-\sin q_{2i-1}, \cos q_{2i-1}]^T, \tag{1}$$

$$P_{4i} = P_{4(i-1)} + l_{b_i}[-\sin q_{2i-1}, \cos q_{2i-1}]^T, \tag{2}$$

where r_i indicates the CoG position of the body segment. The kinetic energy $\mathcal{T}$ and the potential $\mathcal{U}$ are given as follows:

$$\begin{aligned}\mathcal{T} = \frac{1}{2}\sum_{i=1}^{N}\Big\{ & (I_{b_i}^G + d_{2i-1})\dot{q}_{2i-1}^2 + m_{b_i}\dot{P}_{g_{2i-1}}^2 \\ & + k_{2i-1}q_{2i-1}^2 + I_{l_i}^G\dot{q}_{2i}^2 + m_{l_i}\dot{P}_{g_{2i}}^2\Big\},\end{aligned} \tag{3}$$

$$\mathcal{U} = \sum_{i=1}^{N}\left(m_{b_i}P_{g_{2i-1,2}} + m_{l_i}P_{g_{2i,2}}\right)g, \tag{4}$$

where $P_{g_{*,2}}$ is the second component of P_{g_*}, and k_{2i-1} and d_{2i-1} are the spring and viscosity coefficients for the ith body segment. For the leg, there are no spring and damper. Using Lagrangian $\mathcal{L} = T - U$, the equation of motion for the $2N$-link model by Lagrange method is then given as the following:

$$J(q)\ddot{q} + C(q,\dot{q})\dot{q} + D\dot{q} + Kq = \Gamma, \tag{5}$$

where J, C, D, and $K \in R^{(2N+2)\times(2N+2)}$ are the inertial matrix, centrifugal-Coriolis forces matrix, viscosity matrix, and stiffness matrix, respectively. $\Gamma \in R^{(2N+2)\times 1}$ is a generalized force.

3.2 Frictional force for propulsion

We assume that the propulsive force is created by frictional forces from when the leg tips touch the ground as the legs crawled. In this case, the direction of a frictional force is opposite to that of slip velocity. The velocity at the contacting leg tip P_{si} (right or left leg:= P_{4i-2} or P_{4i-1}), is represented by $v_{si} = \dot{P}_{si}$. The frictional force is a function of the normal force $F_{P_{si}}$ affecting the leg tip P_{si}. If we introduce a formula for the friction coefficient $\mu(v_{si})$ of the slip velocity, given by an experimental study [15], then the frictional force at the leg tip is given by the following equation:

$$f_{si} = -\frac{v_{si}}{|v_{si}|}\mu(v_{si})F_{P_{si}}, \tag{6}$$

$$\mu(v_{si}) = \mu_0(1 - e^{-a|v_{si}|}), \tag{7}$$

where μ_0 is the maximum friction coefficient, and a is a positive constant.

3.3 Frictional force to generalized force

We introduced the principle of virtual work in order to express the frictional force as the generalized force of the equation of motion. Because the weights of the body segment and the pair of legs are concentrated at the contacting leg tip, P_{si}, the frictional force acts at that point. If δW_{si} represents the variation of work, it follows that

$$\delta W_{si} = f_{si}^T\delta P_{si} \tag{8}$$

for any variation of the leg tip P_{si}. Because the variation of work is equal to the work done by the external force acting on the leg, $2i$th link, $\Gamma_{f_{si}} \in R^{(2N+2)\times 1}$, for any variation of the link system δq, the following equation holds:

$$f_{si}^T\delta P_{si} = \Gamma_{f_{si}}^T\delta q. \tag{9}$$

Therefore, the following also holds for the relationship between the frictional force f_{si} acting on the leg tip of the $2i$th link and the external force $\Gamma_{f_{si}}$ generated by the frictional force:

$$\Gamma_{f_{si}} = \left(\frac{\partial P_{si}}{\partial q}\right)^T f_{si}. \tag{10}$$

Finally, the external force vector $\Gamma_f \in R^{(2N+2)\times 1}$ acting on all of the links generated by the frictional forces is given by the summation of $\Gamma_{f_{si}}$, i.e.,

$$\Gamma_f = \sum_{k=1}^{N}\Gamma_{f_{si}} = \sum_{k=1}^{N}\left(\frac{\partial P_{si}}{\partial q}\right)^T f_{si}. \tag{11}$$

The generalized force of Eq. (5) is the sum of Γ_f and the input torque at the joints $\tau = [0, \tau_2, ..., \tau_{2N}, 0, 0]^T \in R^{(2N+2)\times 1}$. Hence, it can be described by

$$\Gamma = \Gamma_f + \tau. \tag{12}$$

3.4 Leg movement and control

As mentioned previously, a pair of left and right legs is represented by one link. The propulsive force is generated when the leg crawls alternately. The crawling motion is driven by a sinusoidal function, and the leg tip rotating posteriorly contacts the ground and generates a frictional force, namely,

we assume that the masses of the ith body segment and the ith pair of legs are concentrated to the left or right tip of the ith pair of legs depending on the direction of the rotation:

$$F_{P_{si}} = (m_{b_i} + m_{l_i})g,\ P_{si} = \begin{cases} P_{4i-1},\ \dot{\theta}_{2i} \geq 0 \\ P_{4i-2},\ \dot{\theta}_{2i} < 0 \end{cases}, \tag{13}$$

where $\theta_{2i} = q_{2i} - q_{2i-1}$. The desired trajectory of the leg wave is given by

$$\theta_{d_{2i}} = A\sin(\omega t - i\phi) + \pi/2, \tag{14}$$

where A, ω, and, ϕ are the amplitude, the angular frequency of the leg wave, and phase difference, respectively. The legs controlled by PD raw, which is given as following equation, trace the desired trajectory:

$$\tau_{2i} = -K_p(\theta_{2i} - \theta_{d_{2i}}) - K_d(\dot{\theta}_{2i} - \dot{\theta}_{d_{2i}}), \tag{15}$$

where K_p and K_d are the proportional and derivative gains. The input for the body segment τ_{2i-1} is zero.

4 Numerical simulation

In the simulation, the dynamic model has eight pairs of legs, and a body composed of eight segments, i.e., $N = 8$. The links representing the pair of legs and the body segment are of lengths of 0.28 m ($= l_{l_i}$) and 0.144 m ($= l_{b_i}$), respectively, and of the masses 0.36 kg ($= m_{l_i}$) and 0.364 kg($= m_{b_i}$), respectively, which are identical to the physical parameters of the prototype of i-CentiPot 01. The frequency of the retrograde wave for the legs is $\omega = \pi/4$ rad/s, whereas the amplitude and the phase difference are $A = \pi/8$ rad and $\phi = -\pi/4$ rad, respectively. The spring coefficient k_{2i} and viscosity coefficient d_{2i} are 0.02 and 0.02, respectively. We assume that each link is a uniform rod to derive the moment of inertia. The friction coefficient is $\mu_0 = 0.3$ and the positive constant for the friction model is $a = 20$.

Figure 4 shows snapshots of the result of a simulation of locomoting i-CentiPot every 3 or 4 s. The left/right-hand side of the model is the tail/head. The figure starts at 10.7 s, because the gait is transitive at the beginning of the simulation. The red circles located at each leg tip indicate ground contact. According to the figure, the model could locomote to the right-hand side not only with the leg wave, but also through body undulation. To elucidate the relationship between the leg wave and the body undulation, the phase differences of the legs and of body undulation are plotted as shown in the top and the middle subfigures of Fig. 5. The top subfigure shows a snapshot of the gait, whereas the middle subfigure illustrates the phase differences of the legs, indicated by the red line, and the wave of body segments, indicated by the blue line, at the same

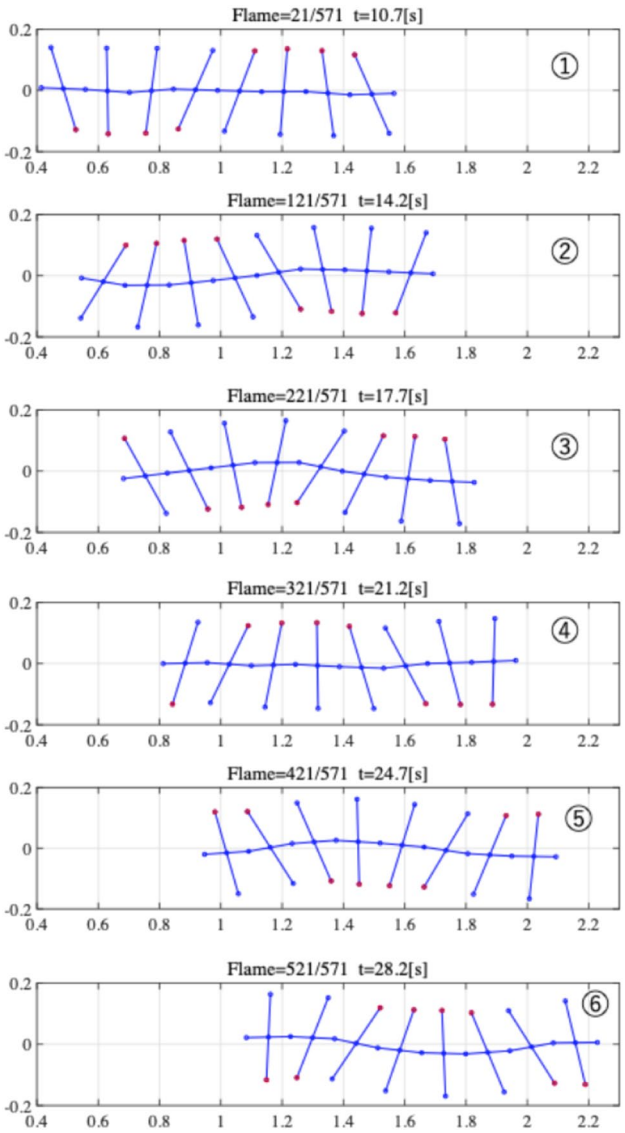

Fig. 4 Result of simulated of locomoting i-CentiPot

time as the snapshot. The body undulation is delayed 1/4 cycle from the leg. The legs concentrated and touched the ground when the red line intersects the abscissa axis from positive to negative. The intersection is around the fourth link, and the fifth joint of the body P_{16} is the vertex at the same position. The body undulation and the leg wave are similar to those of a real centipede and the myriapod robot, i-CentiPot, as mentioned in Sect. 2. The bottom subfigure of Fig. 5 shows a spatiotemporal pattern for the variation in the y axis of the body joints and phase difference of the legs. The yellow signifies a higher value and the dark blue a lower value. The leg wave propagates from head to tail, which indicates a retrograde wave. The body undulation propagates with a phase delay of approximately 1/4 cycle from the leg.

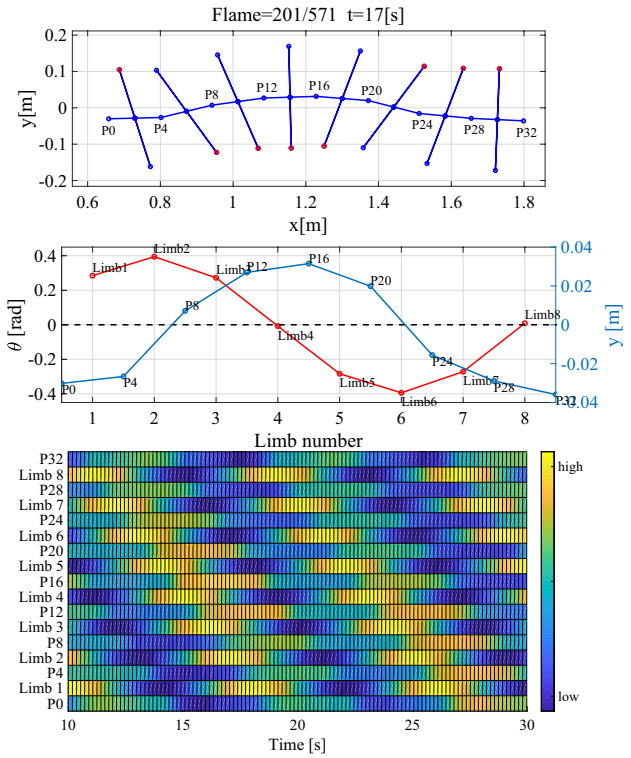

Fig. 5 Snapshot of the gait (top) and phase difference (middle) of the limbs (red line) and a lateral displacement of body undulation (blue line) in the case of $\omega = \pi/4$, and a spatiotemporal pattern of body joints and phase difference of legs (bottom) (colour figure online)

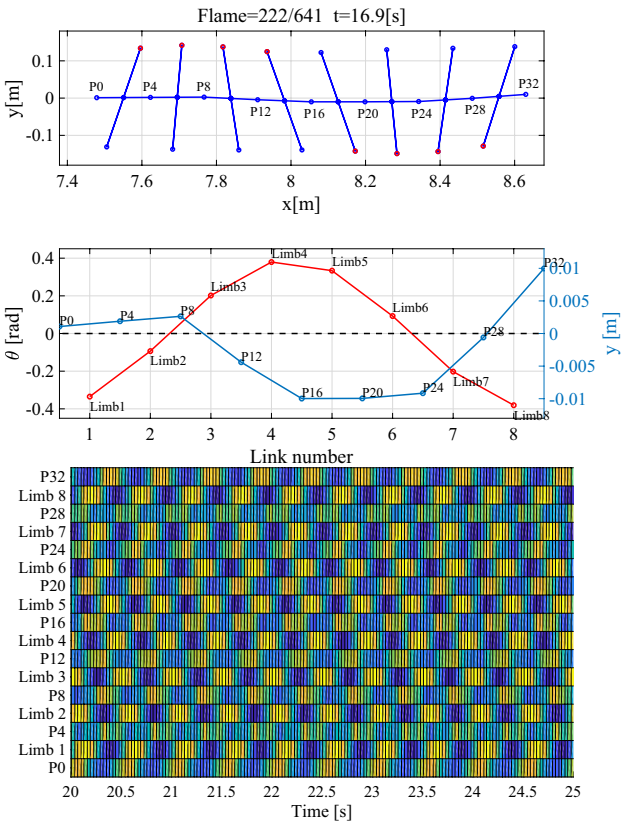

Fig. 6 Snapshot of the gait (top) and phase difference (middle) of the limbs (red line) and a lateral displacement of body undulation (blue line) in the case of $\omega = 4\pi$, and a spatiotemporal pattern of body joints and phase difference of legs (bottom) (colour figure online)

The frequency of the leg wave is increased to 4π, which is much faster than the previous condition. The top and middle subfigures of Fig. 6 show a snapshot of the gait (top) and phase difference and a body undulation (middle) when the frequency of the leg wave is 4π. According to the top subfigure, the body undulates; however, the direction is opposite to that in the previous condition, i.e., the convex area of the body is to the same side of the ground contact as shown in the middle subfigure. The phase difference of the leg intersects the abscissa axis from negative to positive at the third joint P_{12} of the body, which is a vertex in the left-hand side, and vice versa. The body undulation is advanced approximately 1/4 cycle from the leg. This result indicates that the body undulation changes with respect to the frequency of the leg wave. The bottom figure of Fig. 6 shows a time chart for the variation in the y axis of the body joint and phase difference of the legs in the case of 4π. The body undulation propagates with a phase advance of approximately 1/4 cycle from the leg. The frequency of the undulation is faster than in the previous case of $\pi/4$. In other conditions, such as $\omega = \pi, 2\pi$, and 3π, the body undulates as shown in Fig. 7. These figures indicate that the body undulation is reversed between 2π and 3π.

5 Conclusions

In this study, a dynamic model of the myriapod robot, i-CentiPot, was derived to analyze its locomotion, especially to synthesize the body undulation observed for the i-CentiPot and a real centipede. The dynamic model was composed of 16 links, comprising 8 pairs of legs and 8 body segments. The propulsive force was created by the frictional forces at the leg tip.

As a result, the body undulation was synthesized for the retrograde wave of the legs with a frequency of less than 2π rad/s, which was similar to that of a real centipede and i-Centipot. Interestingly, when the frequency increased to more than 3π, the direction of the body undulation was changed to the opposite side of that less than 2π. On the phenomenon in which the body undulation is reversed by the change of the frequency of the leg, there is no report for actual myriapod and robot. The result is an example of the change of the body undulation in the multi-legged agent as the dynamic model with the passive joint of the body, and it is interesting in the sense that it indicates the possibility of the gait other than the currently known gait of centipede.

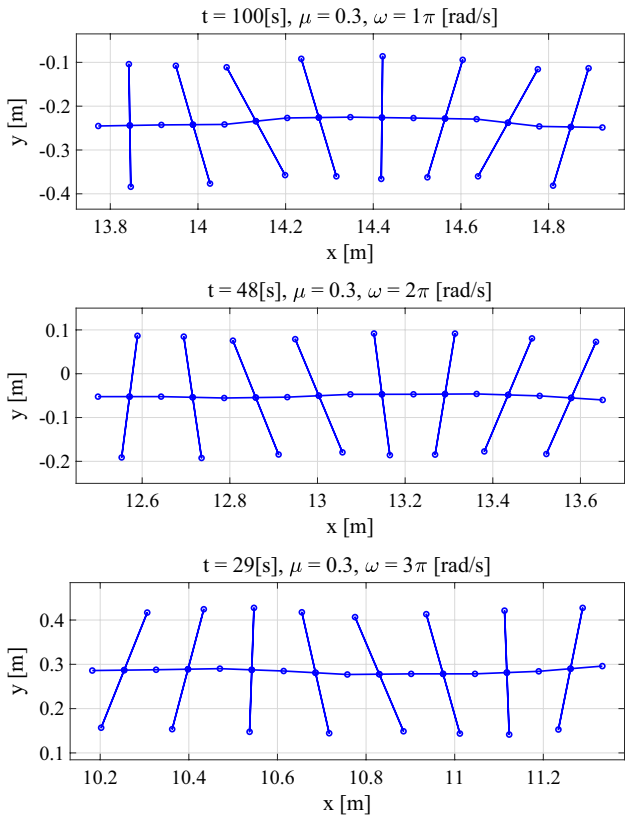

Fig. 7 Body undulation in cases of $\omega = \pi, 2\pi$, and 3π

However, it is not yet clear under what conditions this phenomenon occurs and what it means physically. Therefore, a future challenge is to elucidate the relationship between body undulation and gait in detail.

References

1. Manton S, Harding M (1952) The evolution of Arthropod locomotory mechanisms—Part 3. The locomot Chilopoda and Pauropoda. J Linnean Soc Lond Zool 42(284):118–167
2. Anderson BD et al (1995) Axial kinematics and muscle activity during terrestrial locomotion of the centipede scolopendra heros. J Exp Biol 198:1185–1195
3. Pfeifer Rolf, Bongard Josh (2006) How the body shapes the way we think: a new view of intelligence. A Bradford Book, The MIT Press.
4. Koh D, et al (2010) Centipede robot for uneven terrain exploration: design and experiment of the flexible biomimetic robot mechanism, In: Proc. of the 2010 3rd IEEE RAS & EMB, Intl. Conf. on Biomedical Robotics and Biomechatronics, pp.877-881
5. Saranli U et al (2001) RHex: a simple and highly mobile hexapod robot. Intl J Robot Res 20(7):616–631
6. Hoffman Katie L, Wood Robert J (2011) Passive undulatory gaits enhance walking in a myriapod millirobot. In: 2011 IEEE/RSJ International Conference on Intelligent Robots and Systems, pp.1479-1486
7. Aoi S, Egi Y, Tsuchiya K (2013) Instability-based mechanism for body undulations in centipede locomotion. Phys Rev E 87(1):012717-1-11
8. Aoi S et al (2016) Advantage of straight walk instability in turning maneuver of multilegged locomotion: a robotics approach. Sci Rep 6:30199
9. Kano T et al (2017) Decentralized control mechanism underlying interlimb coordination of millipedes. Bioinspirat Biomimet 12:036007
10. Yasui K et al (2016) On the common decentralized control mechanism underlying centipede and millipede locomotion. Proc. SICE SI Symp 2016:2776–2779
11. Gakken Holdings Co., LTD., Mechamo·Centipede,http://otonanokagaku.net/products/mechanic/centipede/detail.html. Accessed 9 July 2020
12. Osuka K, et al (2017) Development of Implicit Controlled Centipede Robot (i-CentiPot). In:Proc. of SICE Symposium on Decentralized Autonomous Systems:18-23
13. Kiungasa T et al (2017) Development of a small and lightweight myriapod robot using passive dynamics. Artif Life Robot 22(4):429–434
14. Kinugasa T et al (2017) Myriapod Robot i-CentiPot via passive dynamics—emergence of various locomotions for foot movement. In: Proc. of SICE AC 2017
15. Janosi Z, et al (1961) The analytical determination of drawbar pull as a function of slip for tracked vehicles in deformable soils. In: Proc. of ISTVS1st Intl. Conf.: 707-736